View metadata, citation and similar papers at core.ac.uk

brought to you by CORE

provided by University of Strathclyde Institutional Repository

Strathprints Institutional Repository

Summan, R. and Pierce, S.G. and MacLeod, C.N. and Dobie, G. and Gears, T. and Lester, W. and Pritchett, P. and Smyth, P. (2015) Spatial calibration of large volume photogrammetry based metrology systems. Measurement, 68. pp. 189-200. ISSN 0263-2241 , http://dx.doi.org/10.1016/j.measurement.2015.02.054

This version is available at http://strathprints.strath.ac.uk/53441/

Strathprints is designed to allow users to access the research output of the University of Strathclyde. Unless otherwise explicitly stated on the manuscript, Copyright © and Moral Rights for the papers on this site are retained by the individual authors and/or other copyright owners. Please check the manuscript for details of any other licences that may have been applied. You may not engage in further distribution of the material for any profitmaking activities or any commercial gain. You may freely distribute both the url (http://strathprints.strath.ac.uk/) and the content of this paper for research or private study, educational, or not-for-profit purposes without prior permission or charge.

Any correspondence concerning this service should be sent to Strathprints administrator: strathprints@strath.ac.uk

Spatial calibration of large volume photogrammetry based metrology systems

R Summan[1], S G Pierce[1], C N Macleod[1], G Dobie[1], T Gears[2] and W Lester[3], P Pritchett[3], P Smyth[3]

[1] Centre for Ultrasonic Engineering, University of Strathclyde, 204 George Street, Glasgow UK, G1 1XW (rahul.summan@strath.ac.uk)
[2] Hexagon Metrology Ltd, Metrology House, Halesfield 13, Telford UK, TF74PL
[3] Vicon Motion Systems Ltd. Oxford, 14 Minns Business Park West Way, Oxford, OX2 0JB

Abstract. Photogrammetry systems are used extensively as volumetric measurement tools in a diverse range of applications including gait analysis, robotics and computer generated animation. For precision applications the spatial inaccuracies of these systems are of interest. In this paper, an experimental characterisation of a six camera Vicon T160 photogrammetry system using a high accuracy laser tracker is presented. The study was motivated by empirical observations of the accuracy of the photogrammetry system varying as a function of location within a measurement volume of approximately $100m^3$. Error quantification was implemented through simultaneously tracking a target scanned through a sub-volume ($27m^3$) using both systems. The position of the target was measured at each point of a grid in four planes at different heights. In addition, the effect of the use of passive and active calibration artefacts upon system accuracy was investigated. A convex surface was obtained when considering error as a function of position for a fixed height setting confirming the empirical observations when using either calibration artefact. Average errors of 1.48 mm and 3.95 mm were obtained for the active and passive calibration artefacts respectively. However, it was found that through estimating and applying an unknown scale factor relating measurements, the overall accuracy could be improved with average errors reducing to 0.51 mm and 0.59 mm for the active and passive datasets respectively. The precision in the measurements was found to be less than 10 μm for each axis.

1. Introduction

A number of commercially available multi-camera real time photogrammetry systems [1, 2, 3], are used extensively in applications such as gait analysis [4], animation in the entertainment industry [5] and increasingly as tracking systems in robotics [6, 7, 8, 9]. The technique is attractive due to the associated benefits of fully non-contact sensing, six degree-of-freedom (6 DOF) measurement, high temporal sampling rates (up to kHz frequencies), multiple simultaneous object tracking (up to 1000's) and the potential for high accuracy and precision measurements. The accuracy of such systems is dependent upon numerous variables such as the number and resolution of cameras deployed, the dimensions of the measurement volume, the positional configuration of cameras around the measurement volume and the accuracy of the intrinsic and extrinsic parameters computed from the calibration procedure for each camera.

A detailed review of the instrumental errors associated with all the above aspects was provided by Chiari et al [10]. To date, detailed accuracy studies have focused upon relatively small volumes typical of some biomechanical applications. Due to the small measurement volumes involved it has been possible to obtain relatively high accuracy/precision tracking. In [11], the authors evaluate a Vicon MX system composed of five F40 (4 MP, CMOS) cameras for measurement of bone deformation in a

400 x 300 x 300 mm^3 volume. Under optimal conditions the absolute error and precision for displacements of 20 μm were 1.2 - 1.8 μm and 1.5 - 2.5 μm. In [12], the authors consider the suitability of a two camera Qualisys ProReflex-MCU120 (658 x 500 pixels, CCD) for measuring micro displacements of teeth. In a field of view of size 68.18 x 51.14 mm, the accuracy of displacements ranging from 20 - 200μm, was found to be ±1.17%, ±1.67% and ± 1.31% in axis wise terms. The corresponding standard deviations were ±1.7 μm, ±2.3 μm and ±1.9 μm. The authors in [13] present a systematic experiment to determine the static accuracy and precision of a Vicon 460 system composed of five Mcam-60 cameras (1012 x 987 pixels, CMOS). The experiment was conducted for a 180 x 180 x 150 mm^3 volume suitable for the capture of small magnitude biomechanical motion. Dense accuracy measurements were obtained by driving a retro-reflective target affixed to an XYZ scanner (15 μm linear encoder accuracy) to 294 positions according to a 7 x 7 x 6 grid with 30 mm uniform spacing. The influence of several variables was considered: camera positioning around the volume; manual versus scanner based dynamic calibration (controlled arbitrary path); error associated with measurements outside the calibrated volume through calibrating a 90 x 90 x 75 mm^3 sub-volume; marker size and use of lens filtering. Following analysis of the effect of different variable combinations, the optimal set of variables yielded an overall accuracy of 63 ± 5 μm and 15 μm precision. In general it is concluded that major factors in determining overall accuracy include the arrangement of cameras, the marker size (larger markers promoting greater accuracy) and lens filtering to smooth irregular target boundaries. The above studies were confined to small measurement volumes of no more than 0.04 m^3, and errors outside the calibration volume were significantly greater as would be expected. These small measurement volumes are at least 3 orders of magnitude smaller than the present authors' interests where our application for photogrammetry tracking relates to automated robotic inspection [8, 14]. Our research into accurate spatially correlated non-destructive testing (NDT) measurements uses a combination of both mobile semi-autonomous robots [14] and fixed 6 axis industrial robots [15] to deliver NDT measurements to a variety of test samples. The typical measurement volume exceeds 100 m^3 and our applications demand absolute accuracies of significantly less than 1 mm (industrial robot repeatability can routinely attain values of 100s of μm or better over their full working envelope).

Accuracy investigations for larger volumes have typically considered only a small region of the measurement volume [16, 17]. In [16], the authors compare the accuracy of several motion capture systems in a gait analysis context. A subject holding a rigid bar with targets affixed 900 mm apart was instructed to traverse a 3 m linear path through the measurement volume (area 10 m x 6 m). Photogrammetry systems composed of between two and six cameras were used to estimate the length of the bar. In this study, the mean absolute errors varied substantially between 0.53 mm and 18.42 mm. In [18] a "principal points indirect estimate - PIE" approach is reported to provide a rapid calibration approach with an error of 0.37 mm RMS over a volume with a diagonal approximately 1.5 m in length. Accuracy studies for larger volumes, on the scale of 100's m^3, typical of robotics applications have not been reported in the literature. This is surprising as many UAV tracking applications [6] are therefore making unwarranted assumptions about overall system accuracy performance.

There exist a number of commercially available photogrammetry systems for non-contact, high accuracy, measurement of large structures [19, 20] using retro-reflective/white light targets. These systems can provide sub-millimetre accuracy but operate offline. The use of photogrammetry systems in very large scale environments (on the scale of km) is the domain of target-less systems for obvious practicality reasons. Single and multiple camera based systems are used extensively in robotics applications for vehicle pose estimation and environment modelling [21]. Since the target geometry is not known a priori, such systems offer less accuracy than those using targets. Indeed, systems such as that presented in the paper are often used to verify the accuracy of algorithms used by target-less systems.

This article presents a systematic experimental evaluation of the static positional accuracy and precision of a six camera photogrammetry system providing coverage over a 6.8 x 3.8 x 3.8 m (98m^3)

calibrated volume. The error associated with the positional estimates from this system were considered over a measurement volume of dimension 3.9 x 3.05 x 2.3 m^3 (27 m^3) A high accuracy and precision laser tracker Leica absolute tracker AT901B [22] was employed to provide ground truth measurements of the position of a target scanned in four planes dividing the measurement volume vertical height. With reference to the variables identified in [13], an optimal camera arrangement was adopted such that overlap amongst the camera field of views was maximised thus ensuring at least two cameras were available for triangulation at any point in the volume. Dense accuracy measurements were collected inside the calibrated region using large markers of diameter 38.1 mm. The variable of interest in this article centres upon the choice of calibration artefact used for dynamic calibration. The dynamic calibration procedure requires a calibration artefact with known dimensions to be swept through the volume enclosed by the cameras. From the resultant point cloud the relative pose and optical parameters for each camera are determined. These parameters can have significant impact upon system accuracy as they directly affect how a 3D world point is projected onto a 2D image point. Two datasets were collected using different calibration artefacts. The first employed standard retro-reflecting spheres to reflect IR light projected from the cameras, while the second employed actively modulated light emitting diodes (LEDs) to provide active illumination.

The contributions of this paper are threefold: firstly dense spatial measurements over a large volume representative of real robotics applications are reported. Secondly an investigation of the effect of calibration artefact on system accuracy is carried out. Thirdly, an unknown scale factor relating the data from the two systems is identified and subsequently estimated.

2. Experimental methodology for spatial calibration

This section of the paper outlines the experimental approach adopted to make simultaneous measurements between the Vicon motion tracking system and the Leica AT901B laser tracker (used to provide a high accuracy ground truth measurement). Simultaneous measurements were recorded from both systems whilst monitoring a common custom-designed target which was spatially sampled throughout the large measurement volume. A number of specific sub-tasks were identified as being critical to maintaining accuracy of the overall measurement and these are dealt with individually below.

2.1 Vicon motion capture system

The photogrammetry system investigated in this study comprised of a Vicon MX Giganet system [1] the experimental setup of which is illustrated in Figure 1(a) and (b). Six T160 (16 MP with standard Vicon 18 mm focal length lens) cameras were symmetrically arranged at two ends of a rigid frame enclosing a large measurement volume of 98 m^3. The cameras were mounted using professional grade adjustable camera mounts to the smallest sides of a rigid, trussed and braced frame, manufactured from tubing of nominal outside diameter 50 mm. The spatial distribution of the cameras was chosen to maximize the volume of the intersection of the view frustums of the cameras. This resulted in maximizing the number of rays intersecting a marker. The focus and aperture of each camera lens was independently adjusted to ensure optimal intensity and circularity of marker pixel arrays with reference to the standard calibration artefact (colloquially referred to as the “calibration wand”) positioned centrally on the ground plane of the measurement volume. It should be noted that the experiment was conducted in a temperature controlled basement laboratory (±1 °C) environment with a solid concrete floor.

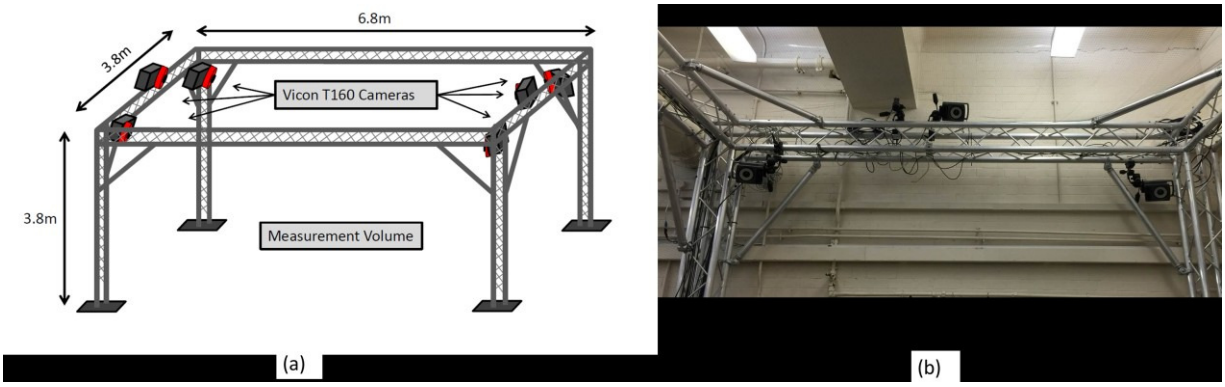

Figure 1 – (a) Positioning of six camera T160 Vicon system around measurement volume (b) Image of real frame

2.2 Photogrammetry system camera calibration

Dynamic calibration [10] is a key step in setting up a precision photogrammetry measurement system. It determines the 3D position and orientation of each camera (the extrinsic parameters) as well as the internal optical and lens distortion parameters (the intrinsic parameters) associated with each camera. The parameters are estimated from the point cloud that results from sweeping a calibration artefact through the volume, with the objective of sampling every part of the volume that will be used during online operation. The error associated with these parameters manifests as a systematic error in the overall accuracy of the system. The importance of these parameters may be understood through the equation mapping a 3D world point, **X**, into a 2D image point on the camera imaging plane, **x**, for a single camera [23]:

$$\mathbf{x} = \mathbf{g}\,(\,K\,[R|\mathbf{t}]\,\mathbf{X}) \tag{1}$$

where K is

$$K=\begin{pmatrix} f & 0 & p_x \\ 0 & f & p_y \\ 0 & 0 & 1 \end{pmatrix} \tag{2}$$

which represents the focal length, f , and the principal point (p_x , p_y). The 3D rotation, R, and translation vector, **t**, of the camera are contained in the matrix [R|**t**] while **g** is the function that removes lens distortion. The two different calibration artefacts used throughout the study are shown in Figure 2.

The passive wand in Figure 2(b) employed standard Vicon 14 mm diameter retro reflectors manufactured by retro-reflective tape wrapping. The active wand in Figure 2(a) utilised actively illuminated LEDs (rather than reflecting the IR light projected from the cameras). The intended advantage of adopting the active artefact lies in the minimisation of the number of partially occluded marker observations and thus outliers captured during calibration. To better understand the variability in parameter estimation between the two calibration artefacts, ten camera calibration trials were undertaken for each wand. In both cases the calibration routine was set to acquire 5000 frames per camera. Due to the size of the volume under consideration, the calibration was carried out manually by sweeping each calibration wand by hand. Although care was taken to minimise variability in volume coverage, the manual approach meant that the exact paths could not be identical. Although the initial expectation was that the active wand would result in smaller standard deviations in the estimated parameters, in practice there was little difference between the calibration techniques. An example of the standard deviation in parameters associated with a single camera is shown in Table 1. The parameters D_0 and D_1 pertain to the lens distortion model and R was converted to the Euler angles θ_x,

θ_y and θ_z. The results show that across ten trials the estimated position of the camera can vary considerably.

Figure 2 - Calibration artefacts, (a) Active calibration Wand (b) Passive calibration wand

Parameter	Unit	Active Wand	Passive Wand
f	Pixels	4561.35 ± 2.33	4559.42 ± 1.74
p_x	Pixels	2414.24 ± 4.29	2417.3 ± 4.05
p_y	Pixels	1736.09 ± 2.35	1732.56 ± 4.52
D_0	N/A	2.56e-9 ± 9.86e-11	2.67e-9 ± 9.99e-11
D_1	N/A	-2.31e-16 ± 2.37e-17	-2.42e-16 ± 1.16e-17
θ_x	Degrees	52.75 ± 0.05	52.77 ± 0.12
θ_y	Degrees	-58.03 ± 0.05	-58.06 ± 0.06
θ_z	Degrees	137.25 ± 0.09	137.29 ± 0.12
X	mm	3624.61 ± 9.16	3609.87 ± 5.33
Y	mm	-1547.15 ± 5.81	-1547.84 ± 8.76
Z	mm	5456.76 ± 6.95	5438.98 ± 3.59

Table 1- Mean and standard deviation in parameters computed from calibration with the active and passive wands

2.3 Ground truth measurement system

In order to evaluate the error associated with Vicon measurements, a system with greater accuracy and precision within the given measurement volume was required. The Leica Absolute Tracker AT901-B [22] is a commercial metrology system capable of providing high accuracy and precise 3D tracking of single targets at a frequency of 1 kHz and ranges of up to 80 m. These systems are commonly employed in the automotive and aerospace industries for aligning and assembling large components. In operation, the 3D position of the centre of a prism retro-reflector is measured through the projection of a laser beam from the instrument to the retro-reflector. Figure 3 shows the location of the laser tracker in the measurement cell. Careful selection of this location was required to enable the tracker to follow the tracked target without an unwanted occlusion of measurement cameras. The tracking system of the laser tracker is composed of two sub-systems; a time-of-flight system for absolute measurements and an interferometer for relative measurements [22]. The time-of-flight subsystem provides a typical-value accuracy of ±10 µm (absolute) while the interferometer provides a typical-value accuracy of ±0.2 µm + 0.15 µm/m [24] (relative). Since only relative measurements were important in this study, over distances not exceeding 6 metres, in all cases the laser tracker provided a maximum distance error of ±1.1 µm.

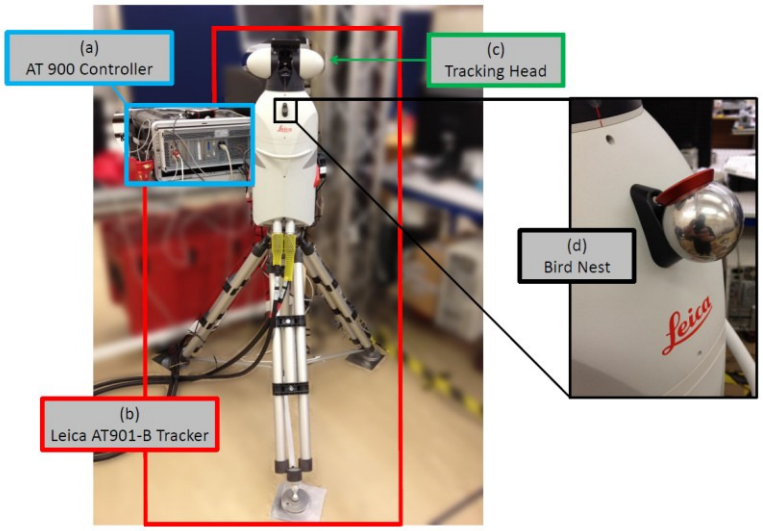

Figure 3 - (a) AT Controller 900 running EmScon software (b) Leica Absolute Tracker AT901-B mounted on heavy duty tripod (c) Tracking head that projects laser (d) Interferometer datum point

2.4 Target Object Design

A fundamental challenge in this study was to devise a test object that both measurement systems could track simultaneously as it was moved throughout the measurement volume. Both systems employed quite different approaches to position measurement; the Vicon system by estimating the centre of a retro-reflecting target from multiple images of the whole target, the Leica tracker through the tracking of a retro-reflective prism. This is in contrast to previous studies that have made use of targets of known lengths with rod-like geometry [16] or have compared relative motions which did not require alignment between the tracking systems [13].

A standard laser tracker target consists of a precision retro-reflector mounted inside a steel spherical shell (a precision machined ball bearing). Standard sizes for the spherical shell are 12.5 mm and 31.8 mm diameters corresponding to imperial sizes of 0.5 and 1.5 inch respectively. By mounting the retro-reflective prism in this fashion, it is possible to position the outer spherical shell into magnetic mounts with a high repeatability (assuming that the magnetic mount surfaces are carefully cleaned of surface debris). This repeatability was evaluated experimentally and it was found that the centre deviation of the reflector over ten trials had a mean value of 3.7 μm per axis. The key to the positioning consistency of the actual retro-reflective prism, lies in the centring accuracy of the prism inside the steel shell. For this study a reflector with the highest level of centring accuracy was selected ($< \pm 0.006$ mm).

The Vicon system could not track the outer shell of the laser tracker target directly, so instead a retroreflective target made from an identical diameter (31.8 mm) steel ball bearing was used. Grade 100 bearings were used with a maximum variation of diameter of 0.0025 mm, and a maximum deviation from spherical form of 0.0025mm as set out in BS ISO 3290-1:2008 [25]. The target was manufactured by wrapping strips of retroreflective tape to the surface of the bearing. The tape which has a thickness of 0.1 mm on a flat surface, introduced an unavoidable systematic error of approximately 0.1 mm per marker. In practice it was difficult to measure this value and therefore account for this in the subsequent analysis. It was considered that this error was negligible compared to the tracking error on the scale of mm which is the focus of this article. It should be noted that the manufacture of markers with a thin layer of retroreflective glass beads (of range 45 – 63 μm diameter) was investigated. The glass beads were bonded to the surface of the ball bearings using a thin layer of adhesive. The use of such retroreflective beads offered the advantage of greater sphericity in

comparison to a wrapped tape version. However, it was found in practice that the resulting markers displayed a higher variation in brightness across the surface than the retroreflective tape based markers – this led to an unwanted potential bias in the centre estimate. In addition, the glass bead retroreflector targets did not reflect IR light as effectively as the tape based markers and there was significant variation in the reflected light across the volume. Given these shortcomings, tape based markers were used for the remainder of the study.

The test object used in the experiment consisted of five magnetic holders mounted upon an aluminium plate. The position of the prism reflector and thus Vicon target centres was initially measured using the AT901 laser tracker and retro-reflective prism target in each holder successively. The four outer targets (A, B, C, D) were used to define a Vicon virtual object (with 6 degree of freedom tracking), and a centre co-incident with the final target (E). In this fashion the (x, y, z) coordinate centre of the Vicon tracked object coincided (to within the tape thickness error) with the centre of the laser tracked retroreflective prism. This approach allowed the simultaneous acquisition of measurement data from both systems. Since the positions of the magnetic mounts were measured on the as-manufactured test object, tolerances such as the flatness of the plate did not contribute error to the method. Figure 4 shows both the real test object and the virtual tracked representation as output from the Vicon tracker system software. It should be noted that the only design constraints on the target were that the photogrammetry system required an object consisting of an asymmetric arrangement of at least four markers and the laser tracker required line of sight to the prism reflector. Any test object satisfying these constraints could be used in this method.

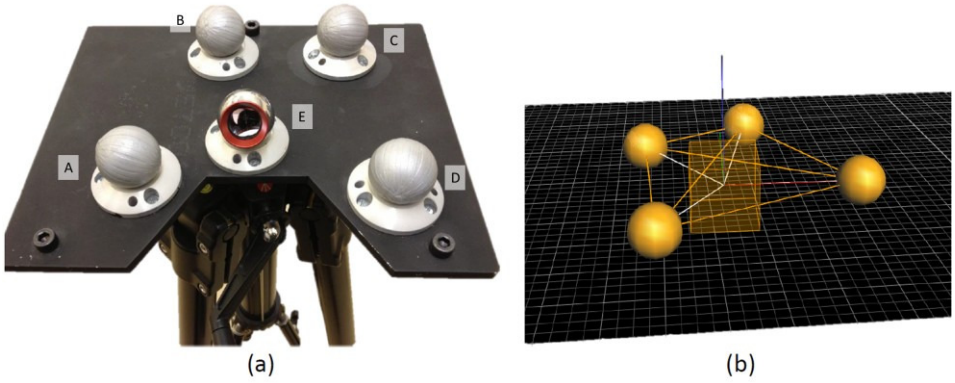

Figure 4 - (a) Object containing coplanar targets (b) Object tracked by Vicon

2.5 Sampling the measurement volume

The target measurements between Vicon and the Leica laser tracker required a method of sampling the position of a target object at multiple positions distributed through the measurement volume whilst maintaining all other system parameters constant. Additionally the adopted method had to maximise target rigidity at each sampling position and also minimise occlusion of the target to the set of observation cameras. Although attractive from a point of view of repeatability and speed of multiple measurements, the use of automated mechanical scanning of the target was not feasible for a number of reasons. Firstly due to the large measurement volume considered in this study, an automated scanner would have required a large working envelope of many 10's metres with the associated rigidity and stability required for the measurements. The physical size of a Cartesian axis scanner implementation would have involved high system integration time and expense, high system mass, and possible target occlusion from the cameras. A six axis robot positioner of sufficient working envelope again would have involved significant engineering integration time and expense, and again have required careful thought to path trajectories to avoid target occlusion with respect to the

measurement cameras. For these reasons a manual approach to the spatial sampling of the measurement volume was adopted. The obvious drawback of the manual approach was the lengthened time required to complete a full set of measurements over the sampled volume. However given the vibrational and thermal stability of the measurement cell as highlighted in section 2.1, it was deemed that the manual approach was satisfactory for the purposes of this investigation.

The adopted approach was to manually translate the custom target object through the measurement volume. The target was mounted on top of a substantial tripod (Manfrotto 161MK2) providing a stable support, minimising target occlusion from the cameras, and allowing for vertical translation of the target object. When scanning a plane the height of the tripod was fixed for all measurements in the plane thus ensuring that the measurements were co-planar to within the planarity of the laboratory floor (1mm deviation recorded by the laser tracker). A series of four vertical positions were considered, and at each height a total of 48 discrete points were measured, making 192 measurement positions in total. Figure 5 shows the eight by six grid measurement grid marked out on the ground plane to aid in sampling the measurement volume at approximately constant intervals.

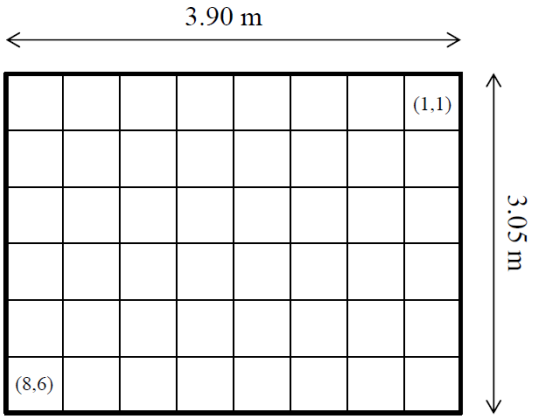

Figure 5 - Grid used to guide acquisition

Custom software was written to obtain co-ordinated measurements from both tracking systems. Two datasets were collected, the first where the Vicon photogrammetry system was calibrated using the passive wand, while the second calibrated the system using the active wand (as discussed in section 2.2). The measurements were captured in four planes 0 ... 3 such that the data for plane 0 was collected at a height of 0.03 m while planes 1- 3 where captured at tripod height settings of 1.06 m, 1.80 m and 2.30 m respectively. At each measurement location 100 measurements were acquired by both systems.

3. Experimental results

3.1 Coordinate frame alignment

Since the measurements were acquired in different system coordinate frames, an alignment procedure was required prior to error analysis. Note that in the following analysis, the use of bar notation denotes a mean data point computed from 100 collected data points. A Vicon measurement, $\overline{\mathbf{V}}_i$, may be expressed in the coordinate frame of the laser tracker as follows:

$$\overline{\mathbf{V}}_i' = sR\overline{\mathbf{V}}_i + \mathbf{t} \tag{3}$$

where, R, is a 3D rotation matrix, $\mathbf{t}$, is the 3D translation vector relating the frame origins, s, is a scaling factor and $\overline{\mathbf{V}}_i'$ is the transformed point. Given N corresponding measurements from both

systems, the transformation parameters R, **t** and s may be recovered through minimisation of the cost function [26]:

$$e^2(R, \mathbf{t}, s)=\frac{1}{N}\sum_{i=1}^{N}\|\bar{\mathbf{L}}_\mathbf{i} -(sR\bar{\mathbf{V}}_\mathbf{i}+\mathbf{t})\|^2 \quad (4)$$

where, $\| \|$, denotes Euclidean distance. Through the inclusion of scale, s, this equation describes a more flexible transformation relating two corresponding point sets. In the following analysis it will be shown that the error vectors computed between the measurements have a particular structure. From our analysis it will be apparent that this structure is best explained by a difference in this scale factor. The analysis, therefore, proceeds in two parts. The first part considers the case where s = 1 which corresponds to processing the raw data produced by Vicon. Given a fixed scale constraint, Equation 4 is minimised as a function of R and **t** using the method described in [27]. The second part considers the more generic case where s is jointly estimated with the rigid body parameters using the minimisation described in [26].

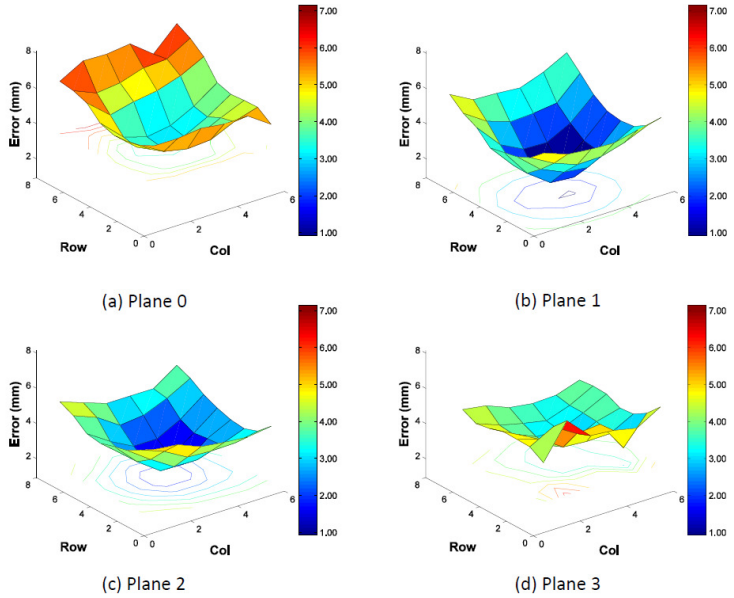

Figure 6 - Error surfaces for each plane using passive wand, scale fixed

In accordance with the grid in Figure 5, the distance error at row, r, and column, c, between a Vicon and laser tracker measurement is calculated as follows:

$$e_{r,c}=\|\bar{\mathbf{V}}'_{r,c}-\bar{\mathbf{L}}_{r,c}\| \quad (5)$$

3.2 Case I: Fixed Scale S = 1

Error as a function of row and column for each layer is shown in Figure 6 for the passive wand and Figure 7 for the active wand. It was found that in general use of the system the errors at the edges of the volume were greater than those at the volume centre. This suggested that the error function would a have a lower value in the centre than the edges. This observation is depicted clearly in the passive wand dataset for planes 0 - 2 and to a lesser extent in plane 3. The error surfaces corresponding to the active wand display similar behaviour particularly in planes 1 and 2. The minimum, mean and maximum errors for each plane are shown in Table 2. Significantly, the errors resulting from the active wand are less than those obtained by calibrating using the passive wand for each plane. The maximum error across the dataset for the passive wand was 7.15 mm while the active wand resulted in a maximum of 4.03 mm. The minimum errors due to the active wand are uniformly sub-millimetre while those for the passive wand vary widely with the worst minimum error being 3.09 mm observed in plane 0. Based upon this data, a system operator could expect an overall mean error of 1.48 mm for the active wand and 3.95 mm for the passive wand.

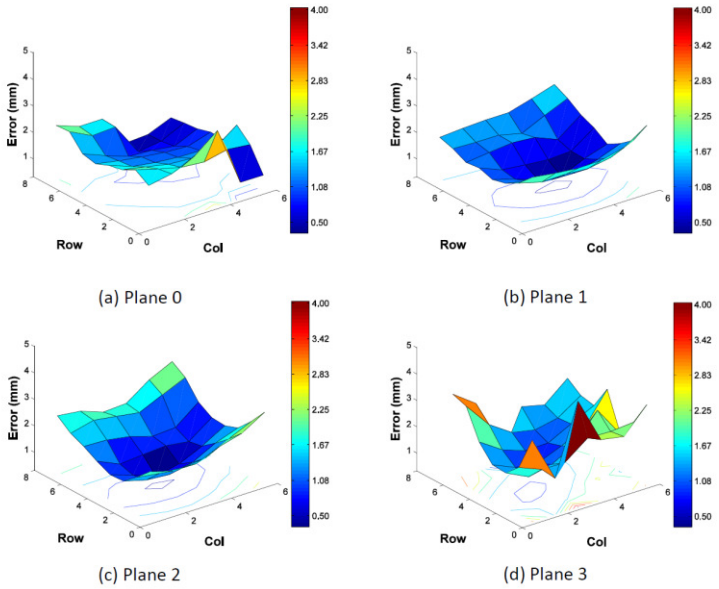

Figure 7- Error surfaces for each plane using active wand where scale is fixed

In order to visualise the spatial error distribution for each calibration artefact, Figure 8 shows a plot of the error vectors at each location. (The arrow heads point toward the true position). Interestingly, the direction of the error vectors for the passive wand are in the opposite direction to those associated with the active wand. Figure 8 (a) suggests that calibration with the passive wand results in the volume being contracted with respect to the true position of the object. The opposite is true in the case of the active wand where the volume is inflated relative to the true position. Estimation of the scale would bring the point clouds into closer alignment motivating the next section.

It should be noted that the precision of the measurement clusters captured at each point of the grid were not affected by the selection of the calibration artefact. The mean axis standard deviations for the passive dataset were σ_x = 4.99 µm, σ_y = 7.64 µm and σ_z = 5.33 µm. Those for the active wand dataset were of similar magnitude corresponding to σ_x = 3.79 µm, σ_y = 5.22 µm and σ_z = 3.65µm. The mean standard deviations in each axis for laser tracker were σ_x = 5.89 µm, σ_y = 2.16 µm, σ_z = 5.18 µm for the passive dataset and σ_x = 5.77 µm, σ_y = 2.18 µm and σ_z = 5.23 µm for the active dataset.

Wand	Plane	Min (mm)	Mean (mm)	Max (mm)
Passive	0	3.09	4.89	7.15
	1	0.93	3.32	5.51
	2	1.67	3.43	4.99
	3	2.99	4.16	6.21
Active	0	0.44	1.29	2.85
	1	0.32	1.28	2.49
	2	0.35	1.48	2.78
	3	0.89	1.88	4.03

Table 2- Minimum, mean and maximum errors with scale fixed to unity

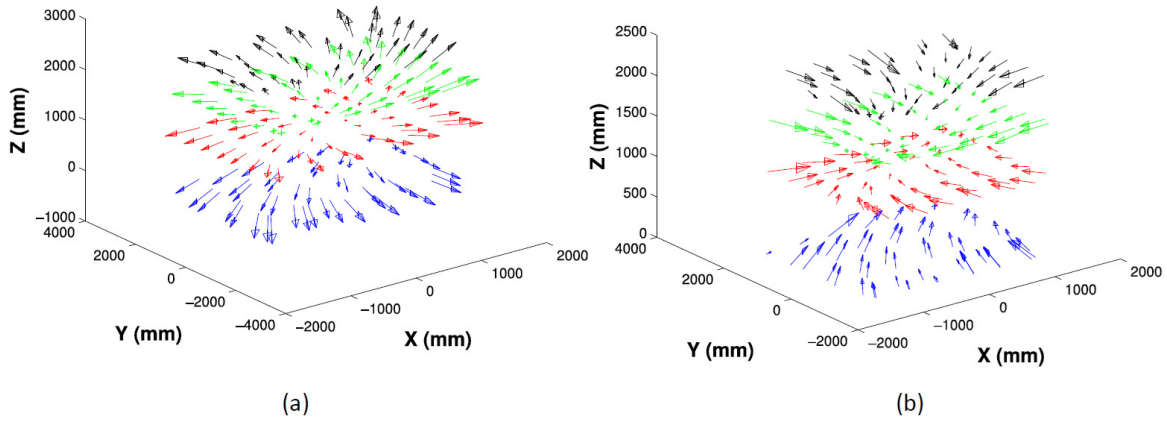

Figure 8-Error vectors with scale fixed (a) Passive Wand (b) Active Wand

3.3 Case II: Scale Estimation

If the cost function in Equation 4 is also minimised as a function of scale factor s, then the measurements may be brought into closer alignment. Using the method in [26], the scale was estimated as s = 1.0025 for the data calibrated with the passive wand while the active wand dataset resulted in a scale of s = 0.9991. The error surfaces resulting from the inclusion of the scale factor are shown for the passive wand in Figure 9 and Figure 10 for the active wand. Notably, the surfaces no longer display a convex like shape; they are more uniform across the volume. In addition to this, the shape of corresponding planes for the two datasets are more correlated than the case of a fixed scale factor. The minimum, mean and maximum errors are shown in Table 3. The maximum error across the

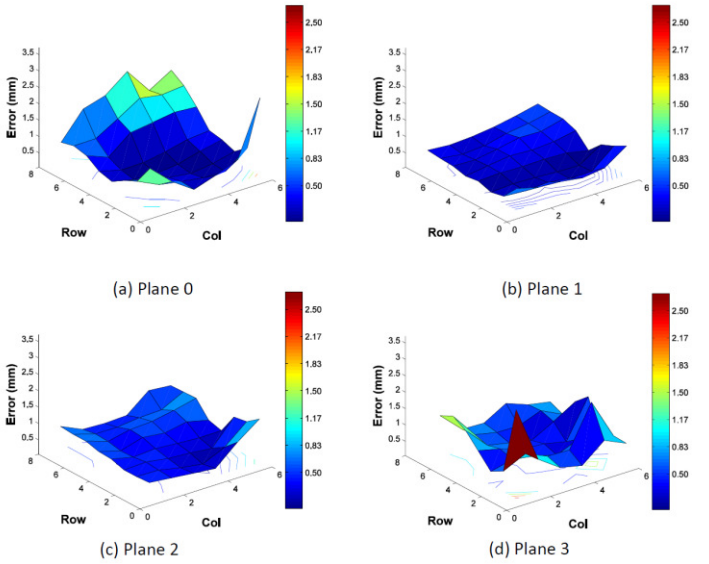

Figure 9 - Error surfaces for each plane using passive wand where scale has been estimated

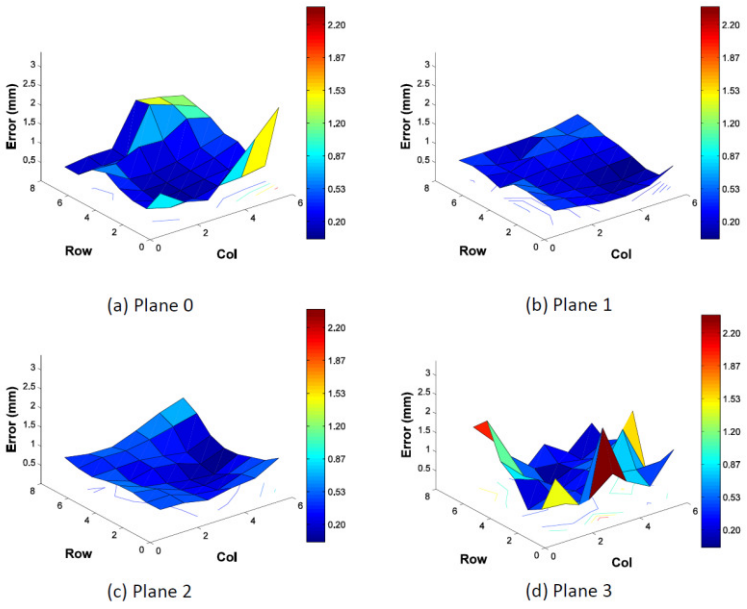

Figure 10 - Error surfaces for each layer using active wand where scale has been estimated

dataset for the passive wand was 2.71 mm while for the active wand it was 2.39 mm. The mean and minimum errors were both sub-millimetre and of similar magnitude. With knowledge of the scale factor, a system operator could expect an overall mean error of 0.51 mm for the active wand and 0.59 mm for the passive wand. Again plotting the error vectors for the scale estimated data sets, (Figure 11) shows that they assume a more stochastic form rather the previously observed contraction/inflation behaviour. Note for both datasets, the standard deviations resulting from the scaled Vicon data can be

obtained by multiplication of the fixed scale case (section 3.2) by the scale factor, s. Therefore, in both cases there is little change in these values.

Wand	Plane	Min (mm)	Mean (mm)	Max (mm)
Passive	0	0.06	0.69	2.36
	1	0.09	0.37	0.89
	2	0.16	0.53	1.32
	3	0.26	0.76	2.71
Active	0	0.06	0.55	2.11
	1	0.03	0.31	0.58
	2	0.05	0.44	1.09
	3	0.09	0.73	2.39

Table 3- Minimum, mean and maximum errors with scale estimated

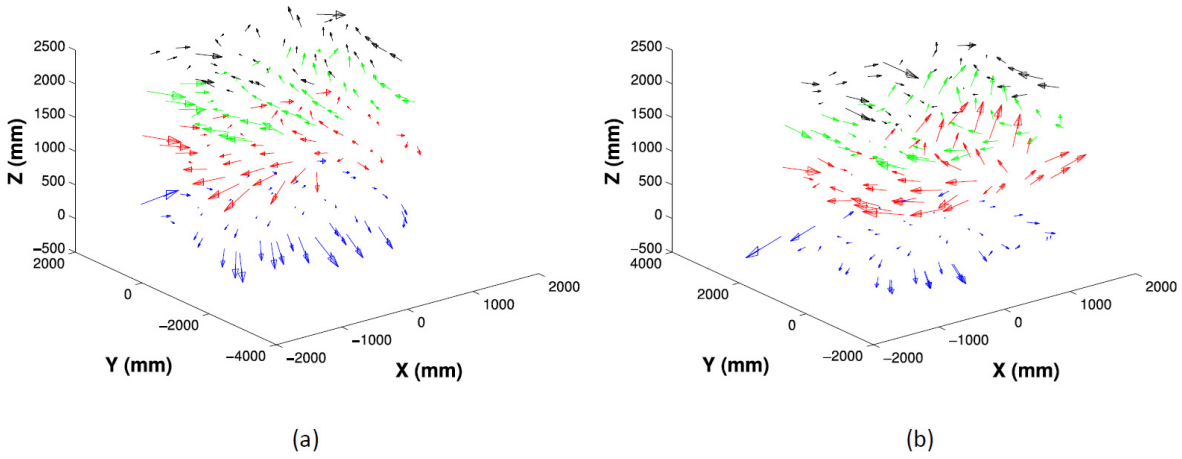

Figure 11 Error vectors with scale estimated (a) Passive Wand (b) Active Wand

4. Discussion

It has been shown that when processing raw Vicon measurements, calibration with the active calibration artefact yielded lower errors than when using the passive wand across the volume investigated. The average errors were 1.48 mm and 3.95 mm for the active and passive datasets respectively for 192 points collected per dataset in a volume of size 3.9 m x 3.05 m x 2.3 m. The magnitude of these errors was in part due to the Vicon measurements being scaled by an unknown factor with respect to the laser tracker data. Through estimation of the scale factor the errors were reduced in both datasets. The values computed for s corresponded to an increase of 0.25% for the measurements in the passive dataset and a reduction of 0.09% in the active dataset. It is possible that such small deviations could be attributed to inaccurate measurements (due to manufacturing tolerances) of marker positions on the calibration artefact (the active or passive calibration wands). Since the calibration routine employed in the photogrammetry software uses the "known" marker configuration to determine the scale applied to measurements in online operation, error in this configuration could propagate into the overall error of the system. However, it should be noted that

the measurement process itself introduces error and thus it may not be possible to entirely attribute scaling error to this effect. Significantly when the scale factor is known, the errors displayed in Table 3 are of a similar magnitude with the average errors becoming 0.59 mm for the passive wand and 0.51 mm for the active wand. Adjustment of the scale factor thus results in a significant reduction in error and makes the difference in calibration artefact type negligible. Direct comparison of current findings with previous studies is made difficult due to differences in hardware and the relative size of the measurement volumes. As discussed in the introduction, most previous studies have concentrated on relatively small measurement volumes consistent with small biomechanical sample measurements. The accuracy with which the centre of the marker is estimated is dependent upon the number of pixels representing the marker in the image. Clearly the greater the number of pixels, the more accurately the shape is captured leading to less error in measuring the centre. Increasing the number of pixels may be achieved by increasing the resolution of the camera or reducing the distance between the marker and camera. Overall the precision of the measurements in each coordinate was less than 10 μm therefore indicating that the photogrammetry system was precise but inaccurate. The systematic nature of the inaccuracy may be mitigated through improving the calibration of the system.

End users of photogrammetry systems for all precision measurement applications should be aware that the magnitude of error associated with measurements is a function of multiple variables including volume size, camera resolution and volume location, as well as calibration approach. General guidance would indicate it would always be prudent to conduct appropriate tests to ensure that the measurement error is within acceptable bounds for the application concerned. Follow up work shall involve the manufacture of a high accuracy calibration artefact to verify the conclusions regarding scale drawn in the analysis.

5. Conclusion

An experimental characterisation of the static positional accuracy and precision of a Vicon T160 photogrammetry system using a high accuracy laser tracker has been presented. The motivation for the study arose through empirical observations of large errors (up to 10 mm) when using robotic measurement systems whose positions were tracked using photogrammetry in a measurement volume of approximately 100 m^3. Precision robotic positioning and control often demands sub-millimetre accuracy motivating significant improvements in the absolute error quantification in this measurement application.

The absolute error of the photogrammetry system was evaluated through simultaneously tracking a target scanned through a 3.9 x 3.05 x 2.3 m^3 measurement volume (27 m^3), and comparing the computed position with the position from the laser tracker. To enable the simultaneous measurements to be undertaken with these two quite different systems required the construction of a custom target. The final target object was mounted on a tripod and measured at each point of a grid of size 8 × 6 and moved through four height settings to generate a set of 192 measurement points. When processing raw data from the photogrammetry system, an error surface was obtained (for a fixed height setting) which displayed lower error in the central region of the volume than the edges - this confirmed empirical observations. It was found that unscaled data mean errors of 1.48 mm and 3.95 mm were obtained for the active and passive techniques respectively (with a maximum observed errors of 4.03mm and 7.15 mm respectively). Through close inspection of our initial experimental findings it became clear that the measurements from both calibration approaches were related by an unknown scale factor. Through estimation and subsequent application of this scale factor, the overall system errors were reduced to 0.51 mm and 0.59 mm for active and passive calibration artefacts respectively.

The main downside of the described approach was the use of tape based markers which lead to an offset between the centring of the laser and photogrammetry targets. However, it was considered that the error introduced by the tape thickness would be much less than that due to tracking inaccuracy. In addition, although care was taken to follow the same path through the volume across experiments during calibration, it was difficult to achieve this exactly in practice.

The approach outlined in this study has enabled a rigorous approach to be established for the calibration of photogrammetry systems for large volume measurement applications (particularly relevant to robotic tracking applications), and additionally provided insight into improved calibration procedures to promote increased measurement accuracy.

6. References

[1] Vicon. 2015. Vicon. [ONLINE] Available at: http://www.vicon.com/ . [Accessed 10 February 15].

[2] Qualisys Motion Capture Systems. 2015. Qualisys. [ONLINE] Available at: http://www.qualisys.com/ . [Accessed 10 February 15].

[3] OptiTrack. 2015. OptiTrack. [ONLINE] Available at:https://www.naturalpoint.com/optitrack/. [Accessed 10 February 15].

[4] Cappozzo A 1984 Gait analysis methodology *Human Movement Science* pp 27–50

[5] Bregler C 2007 Motion capture technology for entertainment [in the spotlight] *Signal Processing Magazine*, *IEEE* pp 160–158

[6] Michael N, Mellinger D, Lindsey Q and Kumar V 2010 The grasp multiple micro-UAV testbed, *Robotics & Automation Magazine*, *IEEE* pp 56–65

[7] Meier L, Tanskanen P, Heng L, Lee G H, Fraundorfer F and Pollefeys M 2012 Pixhawk: A micro aerial vehicle design for autonomous flight using onboard computer vision, *Autonomous Robots* pp 21–39

[8] Dobie G, Summan R, MacLeod C and Pierce S, Visual odometry and image mosaicing for NDE, *NDT & E International*

[9] Kwartowitz DM, Miga, MI, Herrell SD and Galloway RL 2009 Towards image guided robotic surgery: multi-arm tracking through hybrid localization *International journal of computer assisted radiology and surgery* pp 281-286.

[10] Chiari L, Croce UD, Leardini A and Cappozzo A 2005 A Human movement analysis using stereophotogrammetry - Part 2: Instrumental errors, *Gait and Posture* pp 197–211

[11] Yang PF, Sanno M, Brüggemann GP and Rittweger J 2012 Evaluation of the performance of a motion capture system for small displacement recording and a discussion for its application potential in bone deformation in vivo measurements, *Proceedings of the Institution of Mechanical Engineers, Part H: Journal of Engineering in Medicine* pp 838–847

[12] Liu H, Holt C, Evans S 2007 Accuracy and repeatability of an optical motion analysis system for measuring small deformations of biological tissues *Journal of biomechanics* pp 210–214

[13] Windolf M, Gotzen N, Morlock M 2008 Systematic accuracy and precision analysis of video motion capturing systems - exemplified on the Vicon-460 system *Journal of biomechanics* pp 2776–2780

[14] Dobie G, Summan R, Pierce S, Galbraith W and Hayward G 2011 A Non-Contact Ultrasonic Platform for Structural Inspection *IEEE Sensors Journal* pp 2458-2468

[15] Mineo C, Herbert D, Morozov M, Pierce SG, Nicholson PI and Cooper I 2012 Robotic Non-Destructive Inspection *51st Annual Conference of the British Institute for Non-Destructive Testing*

[16] Ehara Y, Fujimoto H, Miyazaki S, Mochimaru M, Tanaka S and Yamamoto S 1997 Comparison of the performance of 3D camera systems II, *Gait & Posture* 5 pp 251–255

[17] Richards JG 1999 The measurement of human motion: A comparison of commercially available systems, *Human Movement Science* pp 589–602

[18] Borghese NA, Cerveri P and Rigiroli P 2001 A fast method for calibrating video-based motion analysers using only a rigid bar *Medical and Biological Engineering and Computing* pp 76–81

[19] Geodetic VStars. 2015. Geodetic Systems inc. [ONLINE] Available at: http://www.geodetic.com/vstars.aspx . [Accessed 10 February 15].

[20] GOM. 2015. ATOS Professional: GOM. [ONLINE] Available at: http://www.gom.com/3dsoftware/atos-professional.html. [Accessed 10 February 15]
[21] Durrant-Whyte, H., & Bailey, T. (2006). Simultaneous localization and mapping: part I. *Robotics & Automation Magazine, IEEE*, 13(2), 99-110.
[22] Leica-Geosystems URL http://www.leica-geosystems.com.
[23] Hartley R and Zisserman A 2000 *Multiple View Geometry in Computer Vision*, vol. 2, Cambridge Univ Press
[24] L. G. M. Products, Leica Absolute Tracker: ASME B89.4.19 Specifications
[25] BS ISO 3290-1: 2008 Rolling bearings *Balls. Part 1. Steel balls*
[26] Umeyama S 1991 Least-squares estimation of transformation parameters between two point patterns *IEEE Transactions on Pattern Analysis and Machine Intelligence* pp 376–380
[27] Arun K, Huang T and Blostein S 1987 Least-Squares Fitting of Two 3D Point Sets, *IEEE Transactions on Pattern Analysis and Machine Intelligence* pp 698–700